

# *P–T–t* evolution of an Early Silurian medium-grade shear zone on the west side of the Famatinian magmatic arc, Argentina: Implications for the assembly of the Western Gondwana margin

B. Castro de Machuca<sup>a,b,\*</sup>, G. Arancibia<sup>c</sup>, D. Morata<sup>d</sup>, M. Belmar<sup>d</sup>, L. Previley<sup>a,b</sup>, S. Pontoriero<sup>b</sup>

<sup>a</sup> CONICET, Argentina

<sup>b</sup> Instituto de Geología, FCEFN, Universidad Nacional de San Juan. Av. Ignacio de la Roza y Meglioli, C.P. 5407 Rivadavia, San Juan, Argentina

<sup>c</sup> Laboratorio Servicio Nacional de Geología y Minería, Avenida Til-Til 1993-Ñuñoa, Santiago, Chile

<sup>d</sup> Departamento de Geología, Universidad de Chile, Plaza Ercilla 803, Santiago, Chile

Received 10 April 2006; received in revised form 30 April 2007; accepted 7 May 2007

Available online 23 May 2007

## Abstract

The geodynamic evolution of the proto-Andean margin of Gondwana during the Paleozoic was characterized by repeated subduction processes associated with the docking of several terranes, including the Cuyania–Precordillera terrane and the Chilenia terrane, and the development of the calc–alkaline Famatinian continental magmatic arc. In the Sierra de La Huerta (30°56′–31°29′ S and 67°17′–67°32′ W), at the southwestern end of the Western Sierras Pampeanas, some mafic to ultramafic igneous bodies belonging to the Famatinian arc were affected by regional metamorphism of the medium-pressure granulite facies (7–7.5 kbar, ≈850 °C). After this regional metamorphism, local mylonitization under amphibolite facies along discrete NW–SE to NNW–SSE striking ductile shear zones occurred. A <sup>40</sup>Ar/<sup>39</sup>Ar plateau age of 432±4 Ma was obtained on rather homogeneous hornblende porphyroclasts from a metagabbro mylonite. The textures and mineral chemistry of the mylonitized metagabbro allow its *P–T–t* evolution from magmatic crystallization to mylonitization to be constrained. Geochronological data obtained from mylonite provide evidence that orogenesis was active at least until the Early Silurian. This deformational event would have been related to uplift and decompression during the later stages of the orogenesis, probably associated with the accretion of the Precordillera terrane to the southwestern Gondwana margin.

© 2007 International Association for Gondwana Research. Published by Elsevier B.V. All rights reserved.

**Keywords:** Metagabbroic mylonites; *P–T* path; <sup>40</sup>Ar/<sup>39</sup>Ar dating; Sierra de La Huerta; Famatinian Orogeny; Argentina

## 1. Introduction

The geodynamic evolution of the proto-Andean margin of Gondwana in Paleozoic times was characterized by repeated subduction processes associated with the docking of several terranes (Ramos et al., 1998; Pankhurst and Rapela, 1998; Rapela et al., 1998; Kleine et al., 2004; Ramos, 2004). In the area of present-day central Chile and central Argentina, the Cuyania (Precordillera) and the Chilenia terranes are considered to have been amalgamated to Gondwana during the Paleozoic (Ramos

et al., 1986; Ramos, 1988; Astini et al., 1995; Thomas and Astini, 1996). The Valle Fértil lineament along the western foothills of the Sierras de Valle Fértil–La Huerta is considered the present eastern boundary of the Cuyania terrane (Introcaso et al., 2004).

Rocks associated with Early Paleozoic subduction activity along the western margin of Gondwana are widely distributed in the west part of the Sierras Pampeanas of central Argentina and are generally referred to as the Famatinian magmatic arc (e.g. Pankhurst and Rapela, 1998; Rapela et al., 1998). The latter lies between the autochthonous Pampean orogen (Mid- to Late Proterozoic–Mid-Cambrian) which constitutes the foreland, on the east, and the allochthonous Precordillera terrane (a “Grenvillian” basement covered by non-metamorphosed to weakly metamorphosed Cambrian–Devonian deposits, Keller et al., 1998) to the west. The arc was developed along the

\* Corresponding author. Instituto de Geología, FCEFN, Universidad Nacional de San Juan. Av. Ignacio de la Roza y Meglioli, C.P. 5407 Rivadavia, San Juan, Argentina. Tel./fax: +54 264 4265103.

E-mail address: [bcastro@unsj-cuim.edu.ar](mailto:bcastro@unsj-cuim.edu.ar) (B. Castro de Machuca).

Gondwana margin during the Early Ordovician and represents the subduction stage that preceded the collision of the Precordillera terrane with the proto-Pacific margin of South America during the Middle Ordovician (Pankhurst et al., 1998).

Previous studies show that the Famatinian arc is a calc–alkaline subduction-related continental magmatic arc that was active between 470 and 490 Ma (e.g. Pankhurst et al., 1998, 2000, and references therein). Regional metamorphism at ca. 460 Ma (Casquet et al., 2001a; Baldo et al., 2001; Rapela et al., 2001; Vujovich et al., 2004) was associated with the collision of the Cuyania terrane. Peak metamorphic conditions reaching the granulite facies were attained (e.g. Baldo et al., 2001) and associated deformation was responsible for the NNW–SSE foliation in the crystalline basement of the Sierras de Valle Fértil–La Huerta and Las Imanas.

After regional metamorphism, local mylonitization along discrete NW–SE to NNW–SSE ductile shear zones occurred in this area (Murra and Baldo, 2001; Castro de Machuca et al., 2004, 2005). According to Murra (2004) this event resulted from uplift and decompression during the later stages of the orogenesis (452–459 Ma), probably associated with the accretion of the Precordillera terrane and representing the last metamorphic event during the construction of the Famatinian arc. The final stage in the evolution of the proto-Andean Gondwana margin consisted of intra-plate magmatism to the east of the arc that took place in Devonian–Carboniferous times (e.g. Dahlquist et al., 2006, and references therein). At this point, the Paleozoic geological development of the Sierras Pampeanas ceased, indicating the stability of the new continental margin, until the start of the Andean cycle in Cretaceous times (Pankhurst and Rapela, 1998).

In this study we focus on mylonites that developed from mafic–ultramafic protoliths cropping out in the Sierra de La Huerta (30°56′–31°29′ S and 67°17′–67°32′ W), at the southwestern end of the Western Sierras Pampeanas (Fig. 1). *P–T* estimations and the <sup>40</sup>Ar/<sup>39</sup>Ar geochronology of this ductile deformation event were determined with the aim of constraining the end of the Famatinian arc-building and, consequently, to improve the geological models proposed for the evolution of the western Gondwana margin.

## 2. Geological setting

The Sierras de Valle Fértil–La Huerta and Las Imanas, the westernmost parts of the Famatinian belt, constitute a morphostructural lineament of pre-Andean high-grade crystalline basement. The latter consists of Upper Proterozoic–Lower Paleozoic metamorphic rocks (metapelitic gneisses, migmatites, marbles and amphibolites), intruded by calc–alkaline metaluminous granodiorites, tonalites, diorites, gabbros, ultramafic rocks and younger granites and pegmatites (Castro de Machuca et al., 1996, and references therein) in Early Ordovician times (468–499 Ma, Pankhurst et al., 2000). Both igneous and metamorphic units were later deformed and transformed into mylonites and ultramylonites along ductile shear zones resulting from a non-coaxial deformation event, showing a retrograde high-grade metamorphic paragenesis of medium-grade minerals

(e.g. Murra and Baldo, 2001; Murra, 2004; Castro de Machuca et al., 2005).

Granodiorites and tonalites are dominant along the eastern flank of the Sierra de Valle Fértil, but lesser amounts of mafic and ultramafic rocks are also found. Tonalites and diorites constitute the more abundant rocks at the eastern side of the Sierra de La Huerta, although gabbroic and ultramafic rocks are locally important. The abundance of intermediate and mafic–ultramafic rocks at the southernmost outcrop could suggest a deeper level (“root”) of exposure of the Famatinian magmatic arc (Castro de Machuca et al., 2002).

Within the Famatinian arc, the different igneous lithologies, including septa of paragneisses, marbles and amphibolites, underwent lower granulite (hornblende–granulite) facies metamorphism. The association of coronitic metagabbros–metagabbrobrorites and ultramafic rocks (peridotites, pyroxenites, hornblendites and lherzolites) with quartz metadiorites, meta-tonalites and metagranodiorites is common (see also Murra and Baldo, 2006, and references therein). Regional metamorphism, with peak *T* at 863–930 °C and *P* between 7–8 kbar (Castro de Machuca et al., 2004), resulted from collision of the Pampia and Cuyania terranes (Chernicoff and Ramos, 2003) and was accompanied by the development of a NNW–SSE penetrative foliation. U–Pb SHRIMP ages on zircon overgrowths indicate a ca. 465 Ma age for the peak of the medium to high-grade regional metamorphism in the area (e.g. Rapela et al., 2001; Baldo et al., 2001; Casquet et al., 2001a; Vujovich et al., 2004). South of the Sierra de La Huerta, a Sm–Nd (Grt+Pl+whole-rock) age of 464.6±4.5 Ma from a migmatitic gneiss (*T*=720–790 °C, *P*=6.5–7 kbar) in the Sierra de Las Imanas, was also interpreted as the age of metamorphism (Galindo et al., 2004). Lower *P–T* values obtained by these authors suggest that the migmatitic gneiss belongs to higher crustal levels than metagabbrobrorites and metagabbros from elsewhere in the Sierra de La Huerta.

Post-regional metamorphism ductile shear zones developed after regional high-grade (granulite facies) protoliths. In the study area, centimetre to meter wide, penetrative NW–SE to NNW–SSE striking mylonite zones (Fig. 1) dip steeply to the NE with a down-dip stretching and mineral lineation (average pitch 85° NW). Displacement in mylonite zones is predominantly reverse but a minor dextral strike–slip component of displacement is also found. Kinematic analysis yields consistent picture of tectonic displacement toward the W–SW. Mylonites are well developed in metagabbroic rocks but also occur in other lithologies. Mylonitic foliation is characteristically defined by the development of mafic and felsic layers (striped texture, Passchier and Trouw, 1996) in spatial transition between coarse-grained undeformed metagabbros and fine-grained mylonitic bands. Layering, foliation and lineation are strongly developed (Fig. 2).

## 3. Sampling and analytical methods

### 3.1. Mineral chemistry

From a total of ninety-six collected samples of undeformed and deformed metagabbros, optical microscope and back-

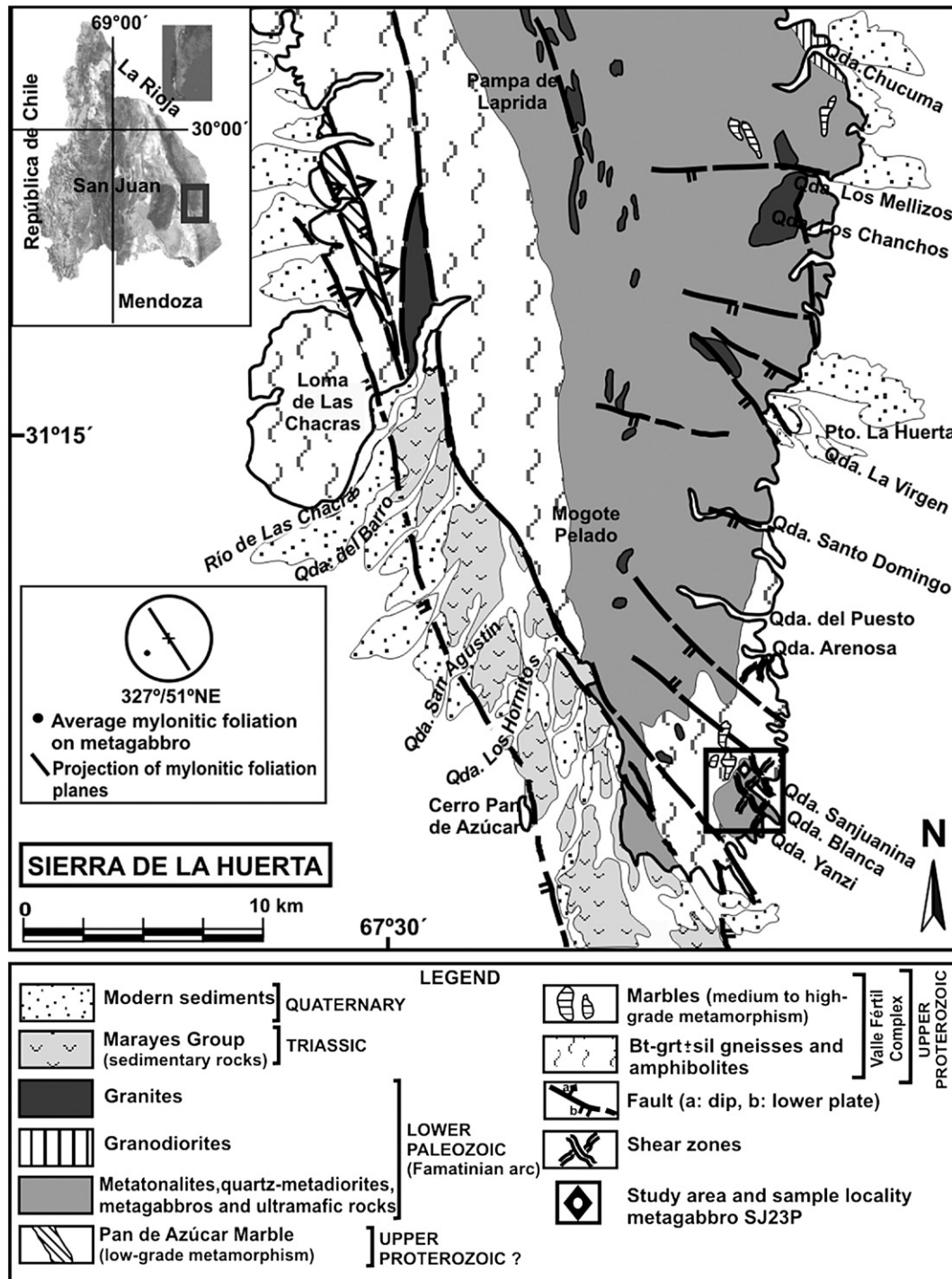


Fig. 1. Simplified geological map of the Sierra de la Huerta showing the location of the study area and dated sample (modified from Vujovich et al., 1996).

scattered scanning electron microscope images were obtained from seven representative oriented sections parallel to the lineation and perpendicular to the foliation (samples BLM9, BLM9b, BM8b, BM7, ARM22, BLM10 and SJ23P). These selected samples were used for microstructural and microprobe studies. Mineral chemistry was determined by electron microprobe analyses (EMPA) on polished and carbon-coated ( $\approx 10$  nm) thin sections. Spot chemical analyses were carried

out in a CAMECA SU-30 SEM-probe (Departamento de Geología, Universidad de Chile, 10 nA, 15 kV, 2  $\mu$ m beam size and 10 s acquisition time). Natural minerals were used as standards and ZAF correction program applied. Previous EMPA data from eight undeformed olivine-bearing metagabbros and ultramafic rocks (samples S1, S2, R6, RSJ14, J14, AR2, R2 and R4, Castro de Machuca et al., 2002) were also used. Representative microprobe analyses are given in Table 1.



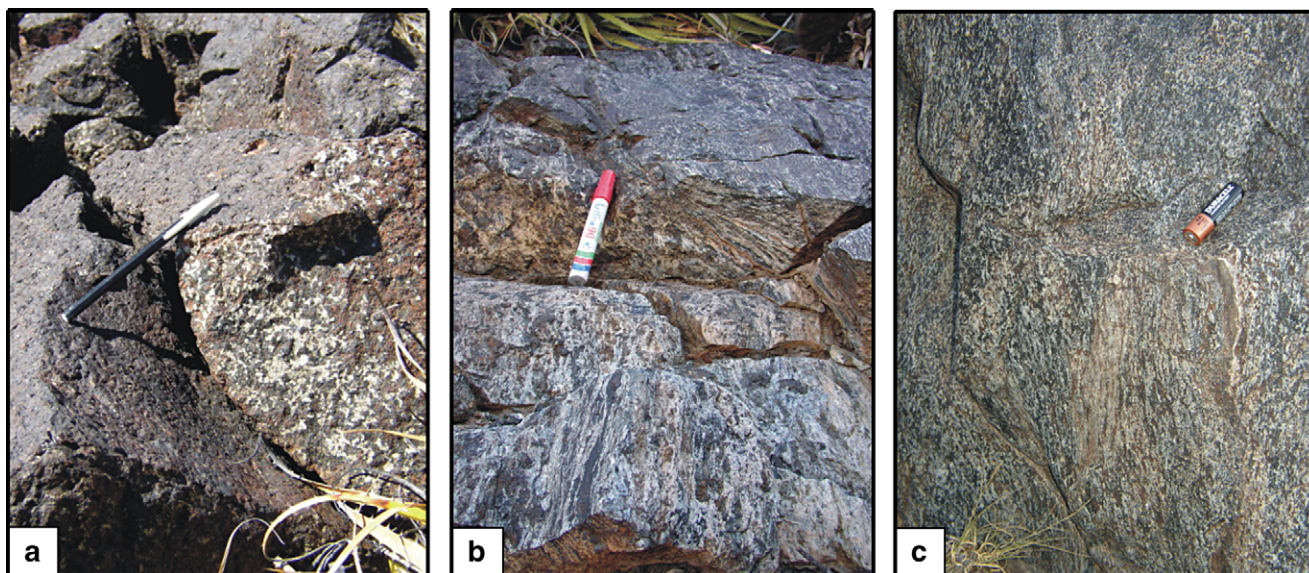


Fig. 2. Sequence of metagabbro outcrops showing a gradation from undeformed coarse-grained metagabbro (a) with increasing deformation to tectonically layered striped metagabbro (b) and intensely deformed fine-grained metagabbro mylonite (c). All photographs are from a NNW–SSE trending ductile shear zone in Quebrada Sanjuanina, southeastern Sierra de La Huerta.

### 3.2. $^{40}\text{Ar}/^{39}\text{Ar}$ procedures

One sample of mylonitized metagabbro (SJ23P) was chosen for  $^{40}\text{Ar}/^{39}\text{Ar}$  dating. Sample preparation and  $^{40}\text{Ar}/^{39}\text{Ar}$  amphibole analysis were carried out in the Laboratorio de Geocronología of the Servicio Nacional de Geología y Minería (Chile). Amphibole was separated by hand picking under a binocular microscope from a 250–180  $\mu\text{m}$  fraction. Separated minerals were cleaned in distilled water for 15 min and dried. Details of analytical procedures and irradiation are given in Arancibia et al. (2006). After irradiation the sample was cooled for three months and the  $J$ -factor value was  $0.001154 \pm 0.0000054$  (Table 2). Blanks obtained during the analysis were as follows:  $^{40}\text{Ar} = 7.42 \times 10^{-17}$ ,  $^{39}\text{Ar} = 4.51 \times 10^{-19}$ ,  $^{38}\text{Ar} = 7.63 \times 10^{-20}$ ,  $^{37}\text{Ar} = 8.13 \times 10^{-19}$ , and  $^{36}\text{Ar} = 2.44 \times 10^{-19}$  mol.

## 4. Petrography and mineral chemistry

### 4.1. Undeformed metagabbros

The mafic–ultramafic bodies associated with the more felsic metaigneous rocks range in size from tens to a few hundred meters, and they are mainly massive, dark-coloured, coarse-grained metagabbros (Fig. 2a). According to modal analyses, these rocks classify as gabbros, gabbro-norites and olivine-bearing gabbro-norites. In the central parts of these bodies, the rocks display well preserved igneous textures and mineralogy and, in some cases, a rhythmic layering is observed. In contrast, marginal parts of the mafic bodies are strongly recrystallized and primary pyroxenes are almost completely replaced by metamorphic amphibole.

The relic igneous mineralogy is formed mainly by subhedral to anhedral rounded grains, up to 4 mm in size, of almost unzoned Mg-rich olivine (Fo<sub>81</sub> to Fo<sub>74</sub>, Table 1), Mg-rich orthopyroxene

( $\approx \text{En}_{77}\text{Fs}_{23}$ ), clinopyroxene ( $\text{En}_{44-47}\text{Fs}_{6-8}\text{Wo}_{50-46}$ ) and subhedral to anhedral anorthite ( $\text{An}_{100-99}$ , Table 1). Pyroxenes are usually clouded with ilmenite–magnetite schiller inclusions. Petrographic relationships indicate a crystallization order of olivine, plagioclase, orthopyroxene and finally clinopyroxene (frequent inclusions of olivine in orthopyroxene and plagioclase in clinopyroxene), consistent with relatively low-pressure crystallization conditions as previously proposed by Rabbia (1996).

As a consequence of metamorphism, abundant coronas of orthopyroxene ( $\text{En}_{82-75}\text{Fs}_{18-24}\text{Wo}_{0-1}$ )  $\pm$  clinopyroxene ( $\text{En}_{47-43}\text{Fs}_{6-8}\text{Wo}_{50-49}$ ) + Al-rich spinel ( $\text{Sp}_{66-43}\text{Hc}_{34-56}$ ) are present at the olivine–plagioclase contacts (Fig. 3a). Spinel is intergrown with clinopyroxene but is also present as single grains. A granoblastic polygonal texture is often found in relic pyroxenes and plagioclase. All these textures are typical of the granulite facies of metamorphism.

Pleochroic pale green tschermakite and tschermakitic hornblende appear at the outermost rim of these coronas in vermicular symplectitic intergrowths with green spinel (Fig. 3a, b), rimming and replacing pyroxenes, as large oikocrysts enclosing previous minerals and as a medium-grained polygonal mosaic in the matrix. Chemically, these amphiboles are characterized by  $\text{Al}_2\text{O}_3$  contents ranging from 13.05–15.88 wt.%,  $\text{Na}_2\text{O}$  from 1.14–2.85 wt.%, and relatively low  $\text{TiO}_2$  (<0.95 wt.%) contents (Table 1). Chemical variations in the amphiboles are dominated by a tschermakitic-type substitution ( $\text{Al}^{\text{IV}} + \text{Al}^{\text{VI}} \leftrightarrow \text{Mg} + \text{Si}$ ).

### 4.2. Mylonites

The transition from undeformed metagabbro to highly deformed mylonite occurs over a distance of only a few centimetres (Fig. 2b and c). The most significant changes resulting from mylonitization are decreasing grain-size and

Table 1

Representative composition of mineral phases in undeformed metagabbros (Mgb) and mylonites (Myl) from the Sierra de la Huerta

Sample	R6	J14	S2	BLM9	SJ23P	SJ23P	R2	J14	R2	BLM9	BLM9	SJ23P	R2	SJ23P	R2
Analysis	3–20	1	2–33	117	3–59	1–82	2–7	7	2–9	114	127	1–63	2–11	3–42	2–1
Mineral	Ol	Ol	Pl	Pl	Pl	Pl	Cpx	Opx	Opx	Cpx	Opx	Opx	Amp	Amp	Spl
Rock	Mgb	Mgb	Mgb	Myl	Myl	Myl	Mgb	Mgb	Mgb	Myl	Myl	Myl	Mgb	Myl	Mgb
SiO <sub>2</sub>	39.28	37.78	41.84	41.68	43.79	52.40	50.53	53.86	53.39	51.26	50.30	50.47	42.41	43.55	FeO
TiO <sub>2</sub>	0.01	0.04	0.00	0.03	0.11	0.00	0.19	0.08	0.02	0.16	0.03	0.05	0.53	0.72	V <sub>2</sub> O <sub>3</sub>
Al <sub>2</sub> O <sub>3</sub>	0.00	0.00	37.16	36.17	36.09	29.43	2.99	1.70	3.06	3.17	4.32	2.00	14.30	11.67	TiO <sub>2</sub>
Cr <sub>2</sub> O <sub>3</sub>	0.00	0.00					0.22	0.14	0.01				0.07	0.00	Al <sub>2</sub> O <sub>3</sub>
FeO	18.66	23.66	0.08	0.02	0.14	0.24	4.08	14.52	13.27	4.39	17.31	23.86	7.84	12.62	MnO
MnO	0.26	0.29	0.00	0.00	0.00	0.18	0.03	0.31	0.23	0.38	0.36	0.69	0.09	0.14	Cr <sub>2</sub> O <sub>3</sub>
MgO	43.62	38.32	0.11	0.02	0.02	0.00	15.89	28.49	29.45	16.40	28.36	21.37	16.10	13.53	MgO
CaO	0.06	0.09	20.49	20.97	19.20	11.72	24.59	0.37	0.48	24.88	0.31	0.32	12.49	11.98	SiO <sub>2</sub>
Na <sub>2</sub> O	0.40	0.00	0.11	0.07	1.28	4.95	0.00	0.00	0.00	0.06	0.02	0.13	1.73	1.27	CaO
K <sub>2</sub> O	0.00	0.00	0.00	0.02	0.05	0.07	0.00	0.00	0.00	0.00	0.00	0.01	0.52	1.23	
SUM	102.29	100.18	99.79	98.97	100.68	98.98	98.52	99.47	99.91	100.71	101.01	98.90	96.08	96.71	SUM
N. Ox	4	4	8	8	8	8	6	6	6	6	6	6	23	23	32
Si	0.983	0.989	1.950	1.962	2.019	2.401	Si	1.874	1.936	1.894	1.858	1.783	1.907	6.102	6.384
Ti	0.000	0.001	0.000	0.001	0.004	0.000	Al <sup>IV</sup>	0.126	0.064	0.106	0.135	0.181	0.089	1.898	1.616
Al	0.000	0.000	2.041	2.007	1.961	1.589	Ti	0.005	0.002	0.001	0.004	0.001	0.001	0.057	0.079
Cr <sup>3+</sup>	0.000	0.000	0.000	0.000	0.000	0.000	Al <sup>VI</sup>	0.005	0.008	0.022	0.000	0.000	0.000	0.528	0.402
Fe <sup>2+</sup>	0.390	0.518	0.003	0.001	0.005	0.009	Fe <sup>3+</sup>	0.104	0.049	0.082	0.143	0.253	0.103	0.819	0.699
Mn <sup>2+</sup>	0.006	0.006	0.000	0.000	0.000	0.007	Cr	0.006	0.004	0.000	0.000	0.000	0.008	0.000	Cr
Mg	1.627	1.495	0.008	0.001	0.001	0.000	Fe <sup>2+</sup>	0.024	0.389	0.315	0.000	0.271	0.657	0.125	0.848
Ca	0.002	0.003	1.023	1.058	0.948	0.575	Mn <sup>2+</sup>	0.001	0.009	0.007	0.012	0.011	0.022	0.011	0.017
Na	0.019	0.000	0.010	0.007	0.115	0.440	Mg	0.879	1.526	1.558	0.886	1.499	1.204	3.452	2.955
K	0.000	0.000	0.000	0.001	0.003	0.004	Ca	0.977	0.014	0.018	0.967	0.012	0.013	1.925	1.882
							Na	0.000	0.000	0.000	0.004	0.001	0.009	0.483	0.361
							K	0.000	0.000	0.000	0.000	0.000	0.000	0.095	0.231
Σcat	3.027	3.011	5.035	5.037	5.056	5.026	Σcat.	4.001	4.002	4.003	4.002	4.011	4.007	15.504	15.474
Fo	0.81	0.74	99.06	99.29	88.96	56.43	En	44.276	76.771	78.699	44.329	73.267	60.202		
Fa	0.19	0.26	0.94	0.62	10.76	43.18	Fs	6.481	22.513	20.379	7.330	26.159	39.144		
			0	0.09	0.28	0.39	Wo	49.244	0.717	0.922	48.341	0.574	0.654		

Ol: olivine; Pl: plagioclase; Cpx: clinopyroxene; Opx: orthopyroxene; Amp: amphibole; Spl: spinel.

development of foliation. The latter is defined by alternating mafic and felsic mineral-rich bands that result in a striped structure at mesoscopic and microscopic scales (Figs. 2b and 3b). This compositional layering consists of polygonal pyroxene+amphibole-rich and plagioclase-rich bands 1 cm to 0.5 mm wide (Fig. 3b). According to EMPA data, no major differences are found in pyroxenes and amphiboles from undeformed and deformed metagabbros. Porphyroclasts with

a relic coronitic texture are also found, as evidenced by pyroxene cores rimmed by amphibole±spinel coronas (Fig. 3c). Symplectitic intergrowths of clinopyroxene–spinel, characteristic of undeformed metagabbros, are however very scarce.

Where grain-size reduction is more important, the dominant texture is mylonitic, with a few large elongated porphyroclasts (up to 4 mm Ø) immersed in a very fine-grained matrix (Fig. 3c, d, e, f and g). Clino- and orthopyroxene porphyroclasts mainly

Table 2

<sup>40</sup>Ar/<sup>39</sup>Ar data obtained from amphiboles in metagabbro mylonite (S 31° 23' 43"–W 67° 19' 33") from the Sierra de La Huerta

SJ23P (Amphibole porphyroclasts from mylonitized metagabbro, Quebrada Sanjuanina, Sierra de La Huerta)

Step	Laser power	<sup>36</sup> Ar/ <sup>39</sup> Ar	<sup>37</sup> Ar/ <sup>39</sup> Ar	<sup>38</sup> Ar/ <sup>39</sup> Ar	<sup>40</sup> Ar*/ <sup>39</sup> Ar	Mol <sup>39</sup> Ar	% <sup>40</sup> Ar*	Age (Ma)	(±2σ)
A	5	0.900	10.626	0.066	84.399	0.001	24.10	168.07	4.89
B	10	0.181	8.466	0.050	224.778	0.006	80.90	417.07	1.79
C	12	0.016	7.537	0.085	234.818	0.013	98.10	433.63	1.32
D	14	0.013	8.257	0.074	233.308	0.014	98.50	431.15	1.83
E	16	0.007	7.961	0.078	233.396	0.014	99.30	431.29	0.97
F	18	0.005	8.320	0.091	234.323	0.009	99.50	432.82	1.47
G	20	0.005	8.422	0.081	233.697	0.009	99.60	431.79	1.52
H	25	0.004	8.172	0.077	234.500	0.009	99.70	433.11	1.52
I	30	0.022	8.664	0.072	234.000	0.008	97.40	432.29	1.50

Integrated age=428±4 Ma; J=0.001154±0.0000054.

Plateau age=432±4 Ma (91.1% released gas).

Inverse isochron age=432±2 Ma, n=7.

Data in italics were excluded in isochron analysis. Laser power in watts. <sup>40</sup>Ar\*=radiogenic <sup>40</sup>Ar.